Environmental Science and Pollution Research (2020) 27:25186–25196
https://doi.org/10.1007/s11356-020-08873-3

RESEARCH ARTICLE

Conversion of cotton textile wastes into porous carbons by chemical activation with $ZnCl_2$, H_3PO_4, and $FeCl_3$

Meiling Xia[1,2] · Xiaohou Shao[1,2] · Zhenhua Sun[3] · Zhihua Xu[3]

Received: 16 October 2019 / Accepted: 13 April 2020 / Published online: 28 April 2020

Abstract

In this study, $ZnCl_2$, H_3PO_4, and $FeCl_3$ were used as activating agents to prepare porous carbons (PC-$ZnCl_2$, PC-H_3PO_4, and PC-$FeCl_3$) from cotton textile wastes at a relativity low temperature. The morphology and structure of carbons were characterized by SEM and XRD demonstrating that carbons with porous property were successfully obtained. Textural properties showed that the PC-$ZnCl_2$ possessed the largest specific surface area of 1854.70 m^2 g^{-1} with mesopores domination. Both of micropores and mesopores existed in PC-H_3PO_4. Micropores were well developed in PC-$FeCl_3$, and the proportion of which was the highest. The FTIR and pH_{pzc} analysis indicated that all the carbons had acidic characteristics, and more acid functional groups were appeared on the PC-$FeCl_3$ than others. The different pyrolysis activation paths were proposed by the thermogravimetric analysis, which proved that the addition of activating agents promoted the formation of pores, lowered the pyrolysis temperature of cotton textile wastes, and inhibited the production of volatiles. The results of adsorption kinetics and isotherm revealed that PC-$ZnCl_2$ exhibited the best adsorption capacity of Cr(VI), and chemical adsorption played a significant role. Meanwhile, surface functional groups of porous carbons also participated in the Cr(VI) adsorption via electrostatic interaction and reduction reaction.

Keywords Cotton textile wastes · Porous carbon · Pyrolysis-activation · Adsorption

Introduction

During the last few decades, masses of textile wastes were produced. Among them, the cotton textile wastes accounted for a large part of textile wastes. In 2013, 562 tons cotton textile wastes were produced in China, accounting for 28% of the stock, nevertheless, the comprehensive recovery and utilization rate was only about 15% (Xu et al. 2018a). Many methods were conducted to dispose textile wastes such as direct processing and recycling. The former mainly included landfill, incineration, and composting, while for the latter, mechanical, physical, chemical, and energy recovery methods were also attempted (Karpenya et al. 2009; Wang 2010). However, there were some shortcomings for the abovementioned methods. It was landfill or incineration that might create serious environmental problems by kinds of leachate and greenhouse gases discharging. For the physical method, as-obtained products were low added value and recycling rate, the high technical requirements were bottleneck problems to energy recovery method (Vasconcelos and Cavaco-Paulo 2006). To deal with these problems, recently, using textile wastes as precursors to prepare carbon-based materials was identified and carried out by some scholars both at home and abroad (Acevedo and Barriocanal 2015; Nahil and Williams 2010).

Porous carbon was widely used in the removal of pollutants because of its large specific surface area and excellent adsorption capacity. Though it could be prepared by different

Highlights 1. Cotton textile wastes were used to prepare porous carbon by different activators.
2. $FeCl_3$ was a promising activating agent at a relatively low temperature of 400 °C.
3. Different pore structure of carbons was related to their unique pyrolysis process.

Responsible Editor: Santiago V. Luis

✉ Xiaohou Shao
shaoxiaohou_hohai@126.com

✉ Zhihua Xu
zhihuaxu_usst@126.com

[1] College of Agricultural Engineering, Hohai University, Nanjing 210098, China

[2] Key Laboratory of Efficient Irrigation-Drainage and Agricultural Soil-Water Environment in Southern China, Ministry of Education, Nanjing 210098, China

[3] School of Environment and Architecture, University of Shanghai for Science and Technology, 516 Jungong Rd, Shanghai 200093, China

traditional precursors such as coal, oil, and shell, the raw materials of non-renewable limited their development. As a kind of textile wastes, cotton textile wastes might be the possibility of preparing carbon materials owing to its low price, large amount, and relative high carbon content. For instance, Zheng et al. (2014) got the ACF from cotton woven waste using the H_3PO_4 as activating agent. And Wang et al. (2016) used waste cotton fabrics as precursor and prepared a new functional porous carbon. In the literatures, traditional chemical activating agents were the priority to prepare the carbon-based materials, but in order to obtain pore-rich porous carbon, the pyrolysis temperature were generally designed highly ranged from 600 to 900 °C. Recently, to reduce the cost of preparation of carbonaceous materials, decreasing the pyrolysis temperature received much concern, and low temperature pyrolysis possessed the potential to retain more surface functional groups (Hong et al. 2019; Hotova et al. 2018).

In numerous methods, chemical activation was widely used to prepare porous carbons nowadays. Traditional chemical activating agents included $ZnCl_2$, H_3PO_4, and KOH (Hesas et al. 2013; Özhan et al. 2014; Zhou et al. 2014). Compared with physical activation process, chemical activation was usually used in industry to prepare high quality porous carbon because of its short-time activation, easily controlled reaction and larger specific surface area products (Rodríguez-Reinoso and Molina-Sabio 1992). Among a number of chemical activators, $ZnCl_2$ was widely adopted in actual production for its relatively low activation temperature and low equipment requirement (Şahin et al. 2014). H_3PO_4 was also gradually taken seriously given that the as-prepared porous carbon was strong acidity and contained more oxygen-containing functional groups at the lower activation temperature, which could be used in waste gas and water treatment (Kuppireddy et al. 2014). Recently, $FeCl_3$ was proved to be an excellent emerging activator which could not only participate in the preparation of porous carbon but also allow the iron compounds to load on the sample at the same time (Oliveira et al. 2009). In addition, it was also recognized as a potentially alternative activating agent for $ZnCl_2$ by researchers for its low price and little pollution. However, until now, there were few studies compared the effects of traditional chemical activating agents with novel ones on the pyrolysis of porous carbon at relatively low temperature. Besides, many researches usually more focused on the properties of resultant products, but it was seldom discussed that the course of pyrolysis process by different activating agents.

Herein, traditional activating agents of $ZnCl_2$ and H_3PO_4 as well as novel activating agents of $FeCl_3$ were used to prepare porous carbons from cotton textile wastes. The primary objectives of our study were (1) to compare the differences in physicochemical properties of these porous carbons that obtained at low temperature (400–500 °C), (2) to explore the pyrolysis-activation behavior of cotton textile wastes in the presence of $ZnCl_2$, H_3PO_4, and $FeCl_3$, and (3) to evaluate the adsorption performance of the prepared porous carbons for Cr(VI) in solution. Morphology, structure and surface characterization of porous carbon were investigated through a series of characterizations such as SEM, XRD, BET, and FTIR. Thermal analysis was used to explore the different pyrolysis activation paths of these carbons. In addition, the adsorption kinetics of Cr(VI) were conducted, and law of adsorption was discussed as well.

Materials and methods

Materials

Cotton textile wastes (CTW), mainly containing mixtures of cotton warp and weft yarns scrap from production process, was obtained from Wuxi No.1 Cotton Mill (Jiangsu Province, China). $ZnCl_2$, H_3PO_4, $FeCl_3{\cdot}6H_2O$, HCl, $K_2Cr_2O_7$, H_2SO_4, C_3H_6O, $C_{13}H_{14}N_4O$, and HNO_3 were all analytical reagents and purchased from Sinopharm Chemical Reagent Co. (Shanghai, China). All the solutions were prepared with deionized water (Milli-Q Advantage A10, 18.2 MΩ cm^{-1}, Germany).

Preparation

Five grams of CTW was cut into small pieces around 3 mm in length, and then impregnated with 25 mL solution (30% w/v) of $ZnCl_2$ (H_3PO_4 or $FeCl_3$) for 12 h at 25 °C. After that the pretreated mixtures were placed in drying oven overnight at 60 °C, and then put into a quartz boat and pyrolyzed in the tubular furnace (heating rate of 10 °C min^{-1}) under nitrogen atmosphere (flow rate of 100 mL min^{-1}). The final pyrolysis temperatures were set as 500, 400, and 400 °C for $ZnCl_2$, H_3PO_4, and $FeCl_3$ with the residence time of 1 h. When the reaction finished, the samples were soaked with 100 mL 10% v/v HCl solution for 10 min and then rinsed with deionized water to neutral. Afterwards, the resultant carbons were put into a drying oven at 105 °C for 12 h prior to use. The porous carbons obtained by different activating agents ($ZnCl_2$, H_3PO_4, and $FeCl_3$) and the cotton textile wastes were named as PC-$ZnCl_2$, PC-H_3PO_4, PC-$FeCl_3$, and CTW, respectively.

Characterization

The morphologies of samples were observed by scanning electron microscope (Hitachi, S4800, Japan). The X-ray diffractograms of carbons were obtained in the 2θ range of 5 to 80° with a canning rate of 3°/min by a diffractometer (Bruker, D8 Advance, Germany). Textural properties of all the carbons were detected by an automatic gas adsorption/

desorption measuring instrument (Quantachrome, Autosorb-iQ-2MP, USA). The specific surface areas of the carbons were calculated by Brunauer-Emment-Teller (BET) equation at 77 K, while pore size distributions of which were obtained by DFT method. Meanwhile, both of the microporous surface areas (S_{mic}) and microporous volumes (V_{mic}) for samples were calculated by t-plot method. The FTIR patterns were carried out in the range of 400–4000 cm^{-1} by an infrared spectrum (Thermo Scientific, Nicolet iS10, USA). One gram of carbon was added to 20 mL deionized water, and which was put on a shaker (150 rpm, 25 °C) for 24 h. The pH of suspension was determined and taken as pH_{pzc} (Moreno-Castilla et al. 2000). The processes of mass loss and heat release/absorption of the samples were analyzed from room temperature to 800 °C in N_2 atmosphere by a thermogravimetric analyzer (PerkinElmer, STA 8000, USA).

The mixtures were denoted as CTW-$ZnCl_2$, CTW-H_3PO_4, and CTW-$FeCl_3$, respectively. The yield was defined as the mass ratio of the carbon after acid pickling to CTW, and the equation was shown as follows:

$$Y(\%) = m/M \times 100\% \quad (1)$$

where Y is the yield, M is the mass of CTW(g), and m is the mass of final carbon (g).

The content of iron in PC-$FeCl_3$ was calculated as follows: 0.1 g sample was put into muffle furnace under 600 °C for 2 h and then the residue was digested with 25 mL, 12 mol L^{-1} HCl solution for overnight. The concentration of iron in the solution was detected by ICP-OES (PerkinElmer, Optima 8000, USA).

Adsorption experiments

For the adsorption kinetics studies, 0.1 g of adsorbent was added to 8 centrifuge tubes each containing 50 mL Cr(VI) solution with concentration of 200 mg L^{-1}. The pH values of all solutions were kept at around 2.0. Then, the mixtures were put in a shaker for 10, 30, 60, 120, 240, 480, 720, and 1440 min at 150 rpm, 25 °C. The concentration of Cr(VI) was measured at the wavelength of 540 nm in a visible spectrophotometer (Shanghai Precision Science Instrument Co., Ltd., 723 N, China) by standard method (GB/T 7467-87).

The adsorption capacity of Cr(VI) at different time was calculated by an equation as follows:

$$q_t = (C_0 - C_t)V/m \quad (2)$$

where C_0 and C_t are the initial and different adsorption time concentration (mg L^{-1}), V is the solution volume (L), m is the mass of adsorbent (g), and Q_t is the adsorption capacity of Cr(VI) at different time (mg g^{-1}).

Pseudo-first-order and pseudo-second-order kinetic equations are used to fit the Cr(VI) adsorption processes, which are shown as follows:

$$q_t = q_e\left(1 - e^{-k_1 t}\right) \quad (3)$$

$$q_t = \left(k_2 q_e^2 t\right) \cdot (1 + k_2 q_e t)^{-1} \quad (4)$$

where q_e is adsorption capacity at equilibrium time (mg g^{-1}), q_t is the amount of adsorption at time t (mg g^{-1}), and k_1 and k_2 are adsorption rate constant of pseudo-first-order (min^{-1}) and pseudo-second-order (g mg^{-1} min^{-1}), respectively.

For adsorption isotherm studies, similar procedures were performed, but several initial concentrations of Cr(VI) (ranging from 100 to 1000 mg L^{-1}) were used for different samples. All the samples were taken after 1440 min.

The equilibrium amount of Cr(VI) adsorbed on porous carbons was calculated by an equation as follows:

$$q_e = (C_0 - C_e)V/m \quad (5)$$

The Langmuir and Freundlich isotherm models are used to analyze the Cr(VI) adsorption behavior, which are shown as follows:

$$q_e = (q_m K_L C_e) \cdot (1 + K_L C_e)^{-1} \quad (6)$$

$$q_e = K_F C_e^{1/n} \quad (7)$$

where C_e (mg g^{-1}) is the equilibrium Cr(VI) concentration, q_e (mg g^{-1}) is the amount of Cr(VI) adsorbed at equilibrium, q_m (mg g^{-1}) is the maximum adsorptive capability, K_L (L mg^{-1}) is the Langmuir affinity constant, and n and K_F ((mg g^{-1})(mg L^{-1})$^{-1/n}$) are the Freundlich constants corresponding to the adsorption intensity and capability, respectively.

Results and discussion

Morphology and structure

Scanning electron microscopy

Figure 1 presents the surface morphologies of CTW, PC-$ZnCl_2$, PC-H_3PO_4, and PC-$FeCl_3$. In Fig. 1a, the surface of CTW was smooth without any porous channels and slits. As shown in Fig. 1b, the formation of irregular and discontinuous cracks was obvious in the surface of PC-$ZnCl_2$ owing to the evaporation effect of $ZnCl_2$ during pyrolysis process and the possible developed pores previously occupied by the $ZnCl_2$ which was wiped off in HCl-rinsing steps (Angin 2014; Demiral and Demiral 2008). In Fig. 1c, for PC-H_3PO_4, the characteristics of pores were more regular than that of two other carbons. The ample honeycombs shaped pores with thin

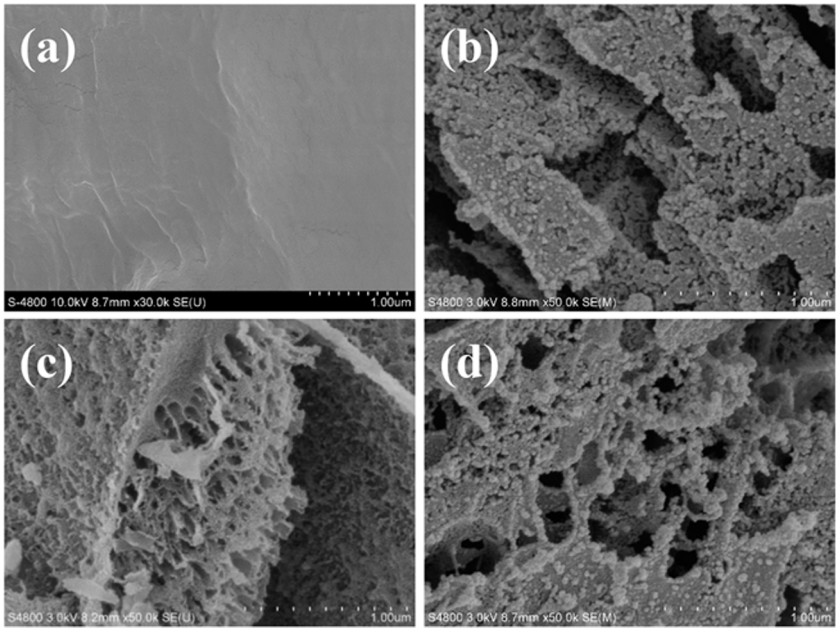

Fig. 1 SEM images of CTW (**a**), PC-$ZnCl_2$ (**b**), PC-H_3PO_4 (**c**), and PC-$FeCl_3$ (**d**)

wall might result from the removal of poly phosphoric acid formed during activation-pyrolysis process, and in which H_3PO_4 mainly acted as a stabilizer to inhibit shrinkage and collapse of carbon structure (Girgis and El-Hendawy 2002; Gonzalez-Serrano et al. 2004). Figure 1d showed that PC-$FeCl_3$ exhibited porous morphology with disorderly and unsystematic pores spread on the surface, and compared with the carbon matrixes mentioned above, whose surface became much rougher by reason of some particles adhering to the edge or filling into the pores, which could be attributed to generation of different iron compounds derived from $FeCl_3$ (Cazetta et al. 2016).

X-ray diffraction

Displayed in Fig. 2 are the XRD images of the porous carbons. The results showed that PC-$ZnCl_2$ and PC-H_3PO_4 had broad peaks at around $2\theta = 25°$ and 43°. And the appearance of wide peak of (002) and tiny peak of (100) belonged to the carbon catalog that could be the incomplete development of microcrystal structure and disorder graphite layers formed during the pyrolysis activation process, respectively (Cazetta et al. 2016; Duan et al. 2017). The values of d_{002} for PC-$ZnCl_2$ (0.363) and PC-H_3PO_4 (0.370) were calculated by Braggs equation, which were larger than that of graphite (d_{002} = 0.340) (Chiu and Ng 2012), indicating the presence of turbostratic carbon structure with randomly oriented graphitic carbon layers (Wang et al. 2009). Particularly, the strong peak intensity of PC-$ZnCl_2$ at 25° confirmed the degree of graphitization was highest. However, the graphite peaks of PC-$FeCl_3$ at 25° and 43° were weak and not even obvious. And the sharp peaks observed at 2θ of 17.26°, 25.00°, and 27.73° could be from the productions of partial decomposition and reaction of cotton textile wastes under the effect of $FeCl_3$ in the relatively low pyrolysis temperature. In addition, the mass of iron content in the PC-$FeCl_3$ remained around 3%, but no distinct peaks were found. It was speculated that different types of iron compounds might trap in or combine with the carbon matrix, then, formed small amorphous or micro-crystalline particles (Fu et al. 2014).

Surface characterization

Textural properties

The N_2 adsorption/desorption isotherms and pores distributions of all carbons are shown in Fig. 3. As shown in Fig. 3a, the adsorption/desorption isotherms of PC-$ZnCl_2$,

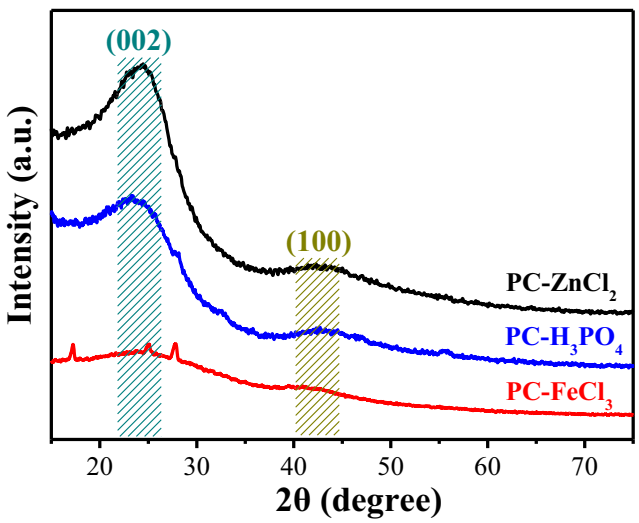

Fig. 2 XRD images of the porous carbons

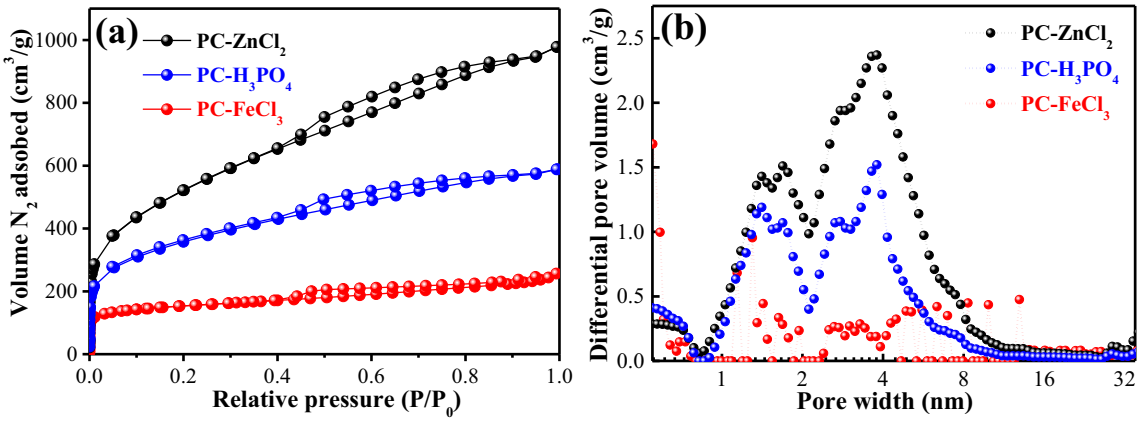

Fig. 3 N_2 adsorption/desorption isotherms (**a**) and pores distributions of porous carbons (**b**)

$PC\text{-}H_3PO_4$, and $PC\text{-}FeCl_3$ all exhibited an intermediate between type I and IV, indicating these samples were mainly combined of microporous and mesoporous structures (Duan et al. 2017). Meanwhile, appearance of type H4 hysteresis loops at the relative pressure of > 0.4 for all carbons was owing to the existence of slit holes (Sing 1985). And as illustrated in Fig. 3b, the pores distribution of $PC\text{-}ZnCl_2$ and $PC\text{-}H_3PO_4$ was similar, which had a relatively broad distribution around 1.5 and 3.5 nm, exhibiting the uniform pores distribution. However, the pores of $PC\text{-}FeCl_3$ were evenly distributed in 0–10 nm without regularity, which was consist with the results of SEM.

Table 1 shows the surface area and pore volume parameters of the porous carbons. The S_{BET} values of $PC\text{-}ZnCl_2$, $PC\text{-}H_3PO_4$, and $PC\text{-}FeCl_3$ were found to be 1854.70 $m^2\ g^{-1}$, 1261.68 $m^2\ g^{-1}$, and 510.20 $m^2\ g^{-1}$, manifesting that activation property of $ZnCl_2$ was the best. As to the $PC\text{-}ZnCl_2$, the S_{ext} and S_{ext}/S_{BET} of which were 1414.99 $m^2\ g^{-1}$ and 76.29%, denoting that $ZnCl_2$ could be beneficial to the formation of mesopores (Angin 2014).

Compared with the others, the $PC\text{-}H_3PO_4$ had the most S_{mic} (469.18 $m^2\ g^{-1}$) and V_{mic} (0.23 $cm^3\ g^{-1}$), along with the smallest average pore diameters (2.89 nm). According to the S_{mic}/S_{BET} (37.19%) and S_{ext}/S_{BET} (62.18%) of $PC\text{-}H_3PO_4$, both micropores and mesopores could be successfully induced during pyrolysis, implying the existence of multiple activation pathways when using H_3PO_4 as activating agent (Carraro et al. 2019; Wong et al. 2018).

Additionally, the S_{mic}/S_{BET} of $PC\text{-}FeCl_3$ was larger than that of $PC\text{-}ZnCl_2$ and $PC\text{-}H_3PO_4$, which occupied 53.67% of the surface area; results showed that $FeCl_3$ as activating agents was conducive to micropores development (Xu et al. 2018b). Meanwhile, the average pore size of $PC\text{-}FeCl_3$ was smaller than that of $PC\text{-}ZnCl_2$, because compared with Zn^{2+}, Fe^{2+} has smaller ionic radius (Oliveira et al. 2009). Moreover, the formation of mesopores might be attributed to the template-like effects of the generated iron compounds (Xu et al. 2020).

Furthermore, the yields of $PC\text{-}FeCl_3$, $PC\text{-}ZnCl_2$, and $PC\text{-}H_3PO_4$ achieved 34.61%, 36.02% and 37.00%, respectively. It was concluded that all the activating agents promoted the development of porous structure in the pyrolysis-activation process, and then the resultant porous carbons of high surface area were obtained with the relatively high yields.

Surface chemistry

Figure 4 displays the FTIR patterns of the carbons. As illustrated in Fig. 4, most peaks of $PC\text{-}ZnCl_2$ were approximate to

Table 1 Surfaces area and pore structure parameters of the porous carbons

Sample	S_{BET}[a] ($m^2\ g^{-1}$)	S_{mic}[b] ($m^2\ g^{-1}$)	S_{mic}/S_{BET} (%)	S_{ext}[c] ($m^2\ g^{-1}$)	S_{ext}/S_{BET} (%)	V_{mic}[d] ($cm^3\ g^{-1}$)	D_p[e] (nm)	Yield (%)
$PC\text{-}ZnCl_2$	1854.70	439.71	23.71	1414.99	76.29	0.20	3.28	34.61
$PC\text{-}H_3PO_4$	1261.68	469.18	37.19	792.50	62.81	0.23	2.89	36.02
$PC\text{-}FeCl_3$	510.20	273.83	53.67	236.37	46.33	0.13	3.11	37.00

[a] The total specific surface area

[b] The micropore specific surface area

[c] The external (mesopores and macropores) specific surface area

[d] The micropore volume

[e] The average pore diameter

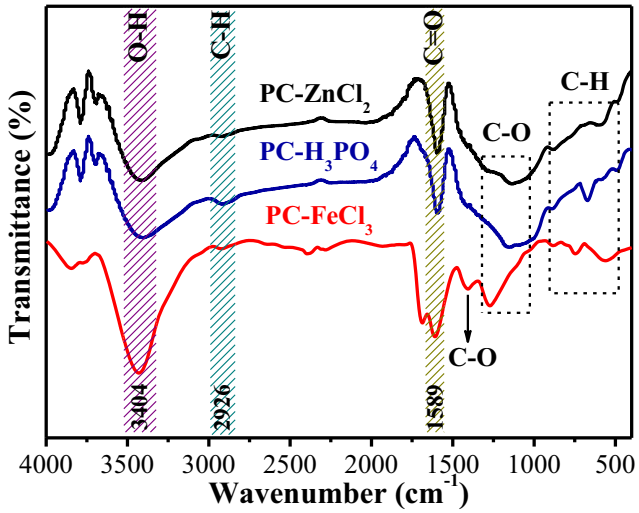

Fig. 4 FTIR patterns of the porous carbons

that of PC-H_3PO_4. The broad bands at 3404 cm^{-1} could be assigned to the –OH stretching vibration of carboxyl and phenol. Bands at 2926 cm^{-1} were owing to the stretching vibration of C–H in –CH–, $–CH_2$, and ——CH_3 and band at 1589 cm^{-1} was attributed to C=O of ketone, aldehyde, and carboxyl (Shouman et al. 2013). The bands about 1000–1300 cm^{-1} could be ascribed to alcohol, phenolic, or carboxyl groups, and the bands located at around 600–1000 cm^{-1} were belong to alkene or aromatic ring structure on the surface of carbons (Kotaiah Naik et al. 2017). When it came to PC-$FeCl_3$, besides the peaks mentioned above, some C=O groups and C–O groups were found at 1685 cm^{-1} and 1414 cm^{-1} (Kotaiah Naik et al. 2017; Suksabye et al. 2007). Moreover, the intensity of band at 3404 cm^{-1} was strongest for PC-$FeCl_3$ due to the more carboxyl and phenol.

Majority groups above on these carbon matrices had acid characteristics leading to the acidic surface (Li et al. 2011). Further research on surface chemistry was carried out through pH_{pzc} testing. The point of zero charges with adsorbents (pH_{pzc}) was a point where an adsorbent has zero potential charge on its surface, which could reflect characters of functional groups on the surface of porous carbon to some extent and show a decreasing rate with the increase of oxygen surface acid groups (Villacanas et al. 2006). The values of pH_{pzc} were 3.08 ± 0.2 for PC-$ZnCl_2$, 2.02 ± 0.2 for PC-H_3PO_4, and 1.96 ± 0.2 for PC-$FeCl_3$, proving that all the carbons were acidic characteristics consisting with results of FTIR (Fu et al. 2014).

Pyrolysis-activation reaction

Thermogravimetric analysis was used to discuss the pyrolysis-activation process of CTW in the present of different activating agents, and the rule of possible pore development was preliminarily expounded. Figure 5 shows the thermogravimetric (TG), differential thermogravimetric (DTG), and differential scanning calorimetry (DSC) spectra of CTW, CTW-$ZnCl_2$, CTW-H_3PO_4, and CTW-$FeCl_3$, respectively.

In Fig. 5a, for CTW, occurrence of mass loss processes was consisted of three stages: (1) The first stage was main moisture removal below 200 °C with 4.8% mass loss. (2) A dramatic mass loss (66.5%) occurred from 250 to 400 °C by the reason of the decomposition of cellulose accompanied with volatile release (Rufford et al. 2011). And the maximum rate of mass loss appeared at 350 °C, which was consistent with the results reported by Shimada et al. (2008). (3) When the temperature

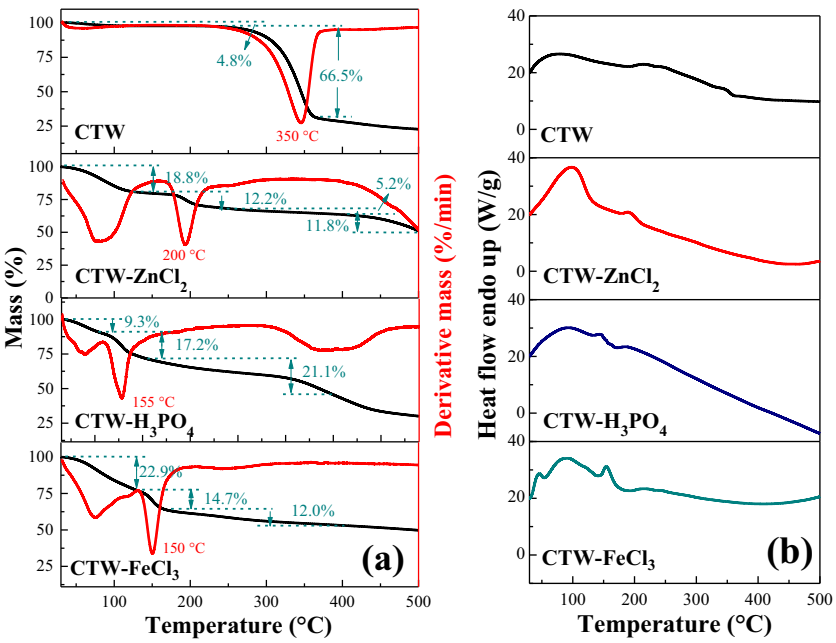

Fig. 5 TG-DTG (**a**) and DSC (**b**) spectra of CTW, CTW-$ZnCl_2$, CTW-H_3PO_4, and CTW-$FeCl_3$

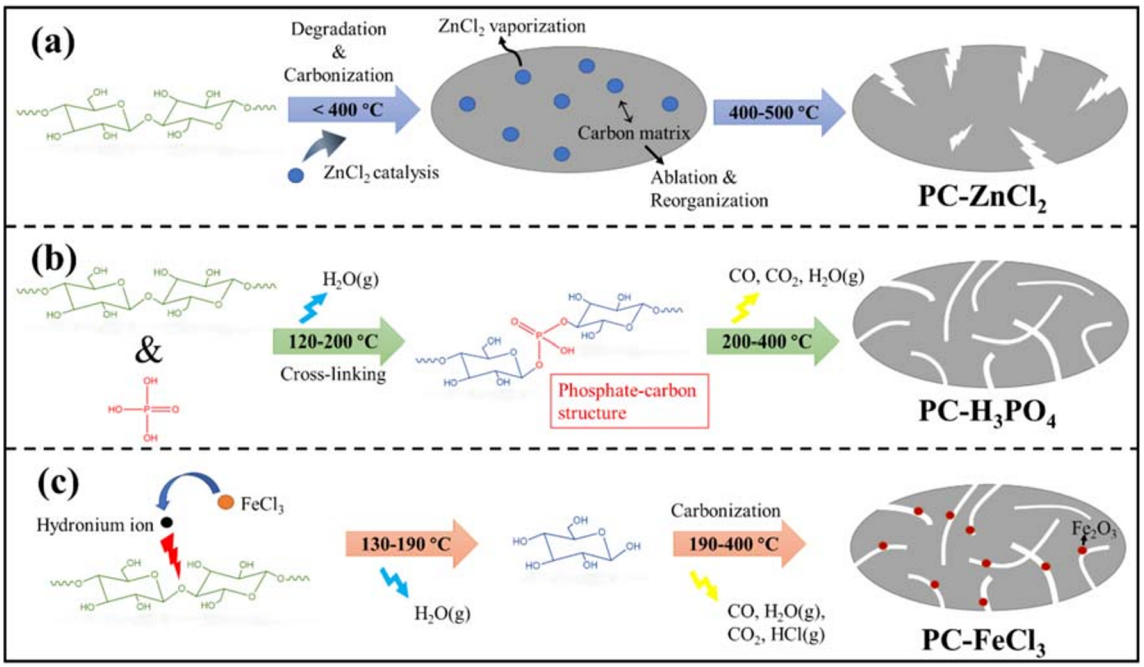

Fig. 6 Schematic diagram on the pyrolysis paths of $ZnCl_2$ (**a**), H_3PO_4 (**b**), and $FeCl_3$ (**c**)

exceeded 400 °C, almost unchanged mass loss happened on account of the stability of solid phase carbide.

For CTW-$ZnCl_2$, mass loss procedures mainly included four stages: (1) The mass loss (18.8%) of CTW-$ZnCl_2$ in the temperature ranged from 0 to 160 °C corresponding to the evaporation of water in CTW and the dehydration effect of $ZnCl_2$, and endothermic reaction appeared on the DSC curve was remarkable in Fig. 5b. (2) In the second stage, the mass loss (12.2%) was shifted to a lower temperature (160–280 °C) in the presence of $ZnCl_2$, which was attributable to the catalytic decomposition of cellulose including hydrolysis, oxidative degradation, and dehydration (Tazibet et al. 2018). Meanwhile, swelling phenomenon occurred along with the lateral bonds breaking in cellulose molecules in $ZnCl_2$ activation, motivating mesopores development (Yahya et al. 2015). (3) The third stage (280–400 °C) was mainly the continuous charring and aromatization processes of the carbon matrix and pore forming, accompany with slight mass loss (5.2%). (4) In the last stage (400–500 °C), there was another obvious mass loss (11.8%) occurred. The carbon matrix was rapidly ablated and restructured due to the vaporization and decomposition of $ZnCl_2$, developing pores by forming interspaces between carbon layers and releasing low-molecular-mass volatile compounds (Xing et al. 2019).

When the temperature was below 120 °C, the mass of CTW-H_3PO_4 lost 9.3% because both of moisture in raw materials and H_3PO_4 was evaporated. During the chemical activation with H_3PO_4, the second stage (120–200 °C) occurred the dehydration and linkages breaking of cellulose, and the precursor of carbon structure formed gradually (Carraro et al. 2019). Sustained mass loss (21.1%) was observed in the range of 200–400 °C, where the cross-link structures in phosphate ester form generated and stable phosphate-carbon structure formed accompanied by large amounts of heat release (Donald et al. 2011). Meanwhile, the generation of volatile compounds (CO, CO_2, H_2O(g) etc.) derived from the reaction between cellulose and H_3PO_4 enhanced the formation of micropores (Xing et al. 2019). Well-developed micropores also have been created through the selective oxidation and erosion of phosphoric acid. On the other hand, the expansion of carbon structure favored the development of mesopores (Wong et al. 2018). The remaining mass of CTW-H_3PO_4 (~ 60%) was higher than that of CTW-$ZnCl_2$ (~ 50%) as to the protection effect of H_3PO_4 for CTW was better than $ZnCl_2$ in the pyrolysis process.

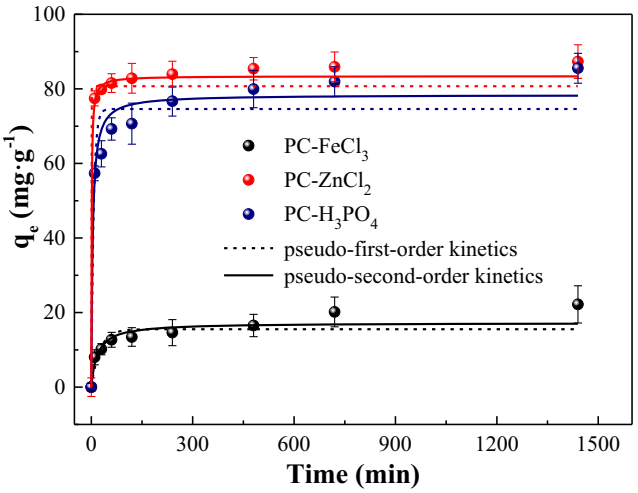

Fig. 7 Adsorption kinetics fitting of Cr(VI) by different porous carbons

Table 2 Fitting parameters of kinetic models for Cr(VI) adsorption by different porous carbons

Sample	$q_{e,exp}$[a]	Pseudo-first-order kinetics model			Pseudo-second-order kinetics model		
	(mg g^{-1})	q_e[b] (mg g^{-1})	k_1[c] (min^{-1})	R^2	q_e (mg g^{-1})	k_2[d] (g mg^{-1} min^{-1})	R^2
PC-$ZnCl_2$	87.31	11.86	0.0030	0.76	86.96	0.0023	0.99
PC-H_3PO_4	85.53	28.83	0.0030	0.90	85.47	0.0007	0.99
PC-$FeCl_3$	22.21	14.89	0.0028	0.96	22.32	0.0007	0.99

[a] The experimental adsorption capacity at equilibrium time

[b] The calculated adsorption capacity at equilibrium time

[c] The adsorption rate constant of pseudo-first-order

[d] The adsorption rate constant of pseudo-second-order

The initial mass loss (22.87%) of CTW-$FeCl_3$ was observed in the range of 0–130 °C on account of the evaporation of free water and crystallization water in CTW along with heat release. In the second stage, the mass loss was (14.7%) shifted to lower temperatures (130–190 °C) accompanied by the endothermic reaction shown in Fig. 5b, as a result of the dehydration of cotton cellulose and early development of volatiles through the interaction between $FeCl_3$ and CTW. $FeCl_3$, as a Lewis acid, could induce the generation of hydronium ion to attack the glycosidic bonds of cellulose, forming numerous glucoses as the precursor of carbon matrix (Xu et al. 2019a). From 190 to 400 °C, with a slight mass loss (12.0%), iron species further evolved (Eqs. (8) and (9)), and carbon structure grew accordingly (Zhu et al. 2014). It should be noted that $FeCl_3$ could inhibit the formation of macromolecular volatiles and conducive to the generation of CO, CO_2, H_2O(g), and HCl(g) (Xu et al. 2019a). Abundant micropores finally developed during the continuous erosion of $FeCl_3$ to CTW and the release of various volatile compounds.

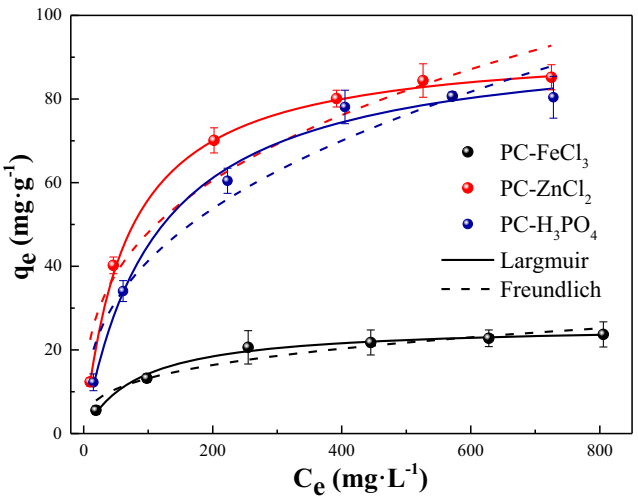

Fig. 8 Adsorption isotherm fitting of Cr(VI) by different porous carbons

$$FeCl3 + 2H2O \rightarrow FeOCl \cdot H2O + 2HCl(g) \rightarrow FeOOH + 3HCl(g) \quad T < 330°C \tag{8}$$

$$2FeOOH \rightarrow Fe2O3 + H2O(g) \quad 380°C < T < 400°C \tag{9}$$

Obviously, the pyrolysis process of CTW inevitably changed with the addition of activators. The maximum weight loss rates of CTW-$ZnCl_2$, CTW-H_3PO_4, and CTW-$FeCl_3$ were 200 °C, 155 °C, and 150 °C, respectively, while that of CTW was 350 °C. In conclusion, the addition of activating agents could reduce the temperature requirement for CTW decomposition, in which the activation effect of $FeCl_3$ was the most significant. And pore formation of these porous carbons was closely related to their unique pyrolysis-activation process. Based on the above analysis, the possible pyrolysis paths of $ZnCl_2$, H_3PO_4, and $FeCl_3$ on CTW pyrolysis were proposed as shown in Fig. 6.

Cr(VI) adsorption

Adsorption kinetics

As exhibited in Fig. 7, the pseudo-second-order kinetics is suitable for the Cr(VI) adsorption for different porous carbons. The adsorption rate had a sharply increase in the first 10 min and slowed down with the lengthening of time. It was reflected that most adsorption sites were mainly distributed on the exterior of the adsorbent and easier to be approached by Cr(VI), thus achieving a more rapid adsorption equilibrium (Yuan et al. 2009). In this process, vacant adsorption sites on the surface of carbons and high solute concentration at the beginning of adsorption process played a key role gradient (Zhang et al. 2015).

As listed in Table 2, the R^2 of pseudo-second-order kinetics of PC-$ZnCl_2$ (0.99), PC-H_3PO_4 (0.99), and PC-$FeCl_3$ (0.99) for Cr(VI) adsorption were relatively larger than that of pseudo-first-order kinetics. Additionally, q_e obtained from

Table 3 Fitting parameters of isotherm models for Cr(VI) adsorption by different porous carbons

Sample	Langmuir			Freundlich		
	q_m[a] (mg g^{-1})	K_L[b] (L mg^{-1})	R^2	n[c]	K_F[d] ((mg g^{-1})(mg L^{-1})$^{-1/n}$)	R^2
PC-$ZnCl_2$	95.12	0.015	0.99	3.01	10.438	0.94
PC-H_3PO_4	93.39	0.009	0.99	2.62	7.144	0.94
PC-$FeCl_3$	26.05	0.012	0.99	3.23	3.175	0.91

[a] The maximum adsorptive capability

[b] The Langmuir affinity constant

[c] The Freundlich constant corresponding to the adsorption intensity

[d] The Freundlich constant corresponding to the adsorption capability

pseudo-second-order kinetic were in close agreement with $q_{e,exp}$, which meant this model was more suitable for fitting the experimental data. In summary, the adsorption processes of all the samples were likely to involve chemical interactions (Cazetta et al. 2016; Sen Gupta and Bhattacharyya 2011). It was notable that the equilibrium adsorption capacity of PC-$ZnCl_2$ (86.96 mg g^{-1}) was close to PC-H_3PO_4 (85.47 mg g^{-1}), meanwhile, larger than that of PC-$FeCl_3$ (22.32 mg g^{-1}). Besides, the rate constant of adsorption (k_2) followed the pattern of PC-$ZnCl_2$ > PC-H_3PO_4 = PC-$FeCl_3$, implying the removal rates of Cr(VI) for PC-$ZnCl_2$ was much faster than that of PC-H_3PO_4 and PC-$FeCl_3$.

Adsorption isotherm

As shown in Fig. 8 and Table 3, Langmuir and Freundlich models were used to further explain the adsorption process. Based on the R^2 values, the Langmuir model was suitable to describe the adsorption of Cr(VI) onto PC-$ZnCl_2$, PC-H_3PO_4, and PC-$FeCl_3$, suggesting that the adsorption process corresponding to monolayer adsorption manner on the homogeneous surface of these porous carbons (Tian et al. 2019). The adsorbed amount of Cr(VI) gradually increased at a lower solution concentration, and then reached the saturated adsorption at a higher equilibrium solution concentration. The adsorption capacity for Cr(VI) of PC-$ZnCl_2$ (95.12 mg L^{-1}), PC-H_3PO_4 (93.39 mg L^{-1}), and PC-$FeCl_3$ (26.05 mg L^{-1}) were comparable to other waste-based carbonaceous adsorbents reported in the literature for Cr(VI) adsorption (Table 4), suggesting the feasibility of employing $ZnCl_2$, H_3PO_4, and $FeCl_3$ as activating agents to prepare cotton textile wastes-based porous carbons for Cr(VI) removal from aqueous solutions.

The large specific surface area and highly porosity of porous carbons provided numerous active sites, which were conductive to the excellent adsorption of Cr(VI) by pore filling (Zhu et al. 2014). Besides, the surface functional groups of porous carbons formed during pyrolysis participated in the Cr(VI) removal as well. Conjectured from the FTIR results, C–H, O–H, C–O, and C=O were widely distributed on carbons surface. O–H groups could be protonated in the strongly acidic solutions and then favored the adsorption performance by combining with the negative $HCrO_4^-$ and $Cr_2O_7^{2-}$ (the main formation of Cr(VI) in solution at pH 2) (Sawalha et al. 2007; Suksabye et al. 2007). During the Cr(VI) adsorption process, C–H on carbons surface was oxidized to C–O and it could be further oxidized to C=O, contributing the reduction reaction from Cr(VI) to Cr(III) at the same time (Xu et al. 2019b). With the most surface functional group content obtained during low temperature pyrolysis, PC-$FeCl_3$ could

Table 4 Comparison of the maximum Cr(VI) adsorption capacities of different adsorbents

Adsorbent	Adsorption capacity (mg g^{-1})	Reference
Combretum quadrangulare Kurz-carbon	1.68	(Maneechakr and Karnjanakom 2017)
Coconut shell-carbon	10.88	(Babel and Kurniawan 2004)
Bamboo bark-carbon	19.53	(Zhang et al. 2015)
Sugar beet pulp-carbon	24.2	(Altundogan et al. 2007)
Terminalia arjuna nuts-carbon	28.43	(Mohanty et al. 2005)
PC-$ZnCl_2$	95.12	This study
PC-H_3PO_4	93.39	This study
PC-$FeCl_3$	26.05	This study

removal Cr(VI) effectively. Meanwhile, these surface functional groups affected the pH_{pzc} of porous carbon. It was generated to know that when $pH_{pzc} > pH$, the net charge on the surface of porous carbon was positive favoring the adsorption of anion, and when $pH_{pzc} < pH$, the net charge on the surface of the porous carbon was negative in favor of the cation adsorption (Faria et al. 2004). Based on values of pH_{pzc}, in comparison to PC-$FeCl_3$, the PC-$ZnCl_2$ and PC-H_3PO_4 had stronger electrostatic adsorption for Cr(VI) adsorption while $HCrO_4^-$ and $Cr_2O_7^{2-}$ were the predominant species at pH 2 (Anandkumar and Mandal 2009).

Conclusion

In this study, morphology, structure, surface characterization, and pyrolysis activation paths of the porous carbons derived from cotton textile wastes by different activating agents ($ZnCl_2$, H_3PO_4, and $FeCl_3$) were confirmed. (1) The cotton textile wastes-based porous carbon possessed with well-developed pore structure, high yield, and high specific surface area through the activation of different activating agents. (2) The PC-$ZnCl_2$ displayed the highest surface area, which could reach 1854.70 $m^2\ g^{-1}$. The PC-H_3PO_4 possessed micro-mesoporous structure, while the proportion of micropores in PC-$FeCl_3$ was the highest. (3) The cotton textile wastes-based porous carbon mainly presented acidic property as a result of the formation of numerous acid functional groups promoting the adsorption of cations and heavy metals. Among them, PC-$FeCl_3$ possesses most acid groups. (4) The activating agents lowered the pyrolysis temperature of cotton textile wastes, inhibited the production of volatiles and promoted the formation of pores. In addition, the differences of pore features were closely related to their unique pyrolysis-activation process. (5) The maximum adsorption capacities of PC-$ZnCl_2$, PC-H_3PO_4, and PC-$FeCl_3$ toward Cr(VI) were 86.96, 85.47, and 22.32 mg g^{-1}, respectively. The adsorption process was mainly involved pore filling, electrostatic interaction, and reduction reaction as to the large surface area and surface functional groups.

Funding information We appreciate the financial support from the National Key Research and Development Program of China (2018YFD0200503), National Natural Science Foundation of China (21707090), and China Postdoctoral Science Foundation (2017M611590).

References

Acevedo B, Barriocanal C (2015) Preparation of MgO-templated carbons from waste polymeric fibres. Microporous Mesoporous Mater 209: 30–37

Altundogan HS, Bahar N, Mujde B, Tumen F (2007) The use of sulphuric acid-carbonization products of sugar beet pulp in Cr(VI) removal. J Hazard Mater 144:255–264

Anandkumar J, Mandal B (2009) Removal of Cr(VI) from aqueous solution using Bael fruit (Aegle marmelos correa) shell as an adsorbent. J Hazard Mater 168:633–640

Angin D (2014) Production and characterization of activated carbon from sour cherry stones by zinc chloride. Fuel 115:804–811

Babel S, Kurniawan TA (2004) Cr(VI) removal from synthetic wastewater using coconut shell charcoal and commercial activated carbon modified with oxidizing agents and/or chitosan. Chemosphere 54: 951–967

Carraro PS, Spessato L, Crespo LHS, Yokoyama JTC, Fonseca JM, Bedin KC, Ronix A, Cazetta AL, Silva TL, Almeida VC (2019) Activated carbon fibers prepared from cellulose and polyester–derived residues and their application on removal of Pb^{2+} ions from aqueous solution. J Mol Liq 289:111150

Cazetta AL, Pezoti O, Bedin KC, Silva TL, Paesano Junior A, Asefa T, Almeida VC (2016) Magnetic activated carbon derived from biomass waste by concurrent synthesis: efficient adsorbent for toxic dyes. ACS Sustain Chem Eng 4:1058–1068

Chiu K-L, Ng DHL (2012) Synthesis and characterization of cotton-made activated carbon fiber and its adsorption of methylene blue in water treatment. Biomass Bioenergy 46:102–110

Demiral H, Demiral İ (2008) Surface properties of activated carbon prepared from wastes. Surf Interface Anal 40:612–615

Donald J, Ohtsuka Y, Xu C (2011) Effects of activation agents and intrinsic minerals on pore development in activated carbons derived from a Canadian peat. Mater Lett 65:744–747

Duan X, Srinivasakannan C, Wang X, Wang F, Liu X (2017) Synthesis of activated carbon fibers from cotton by microwave induced H_3PO_4 activation. J Taiwan Inst Chem Eng 70:374–381

Faria PC, Orfao JJ, Pereira MF (2004) Adsorption of anionic and cationic dyes on activated carbons with different surface chemistries. Water Res 38:2043–2052

Fu K, Yue Q, Gao B, Sun Y, Wang Y, Li Q, Zhao P, Chen S (2014) Physicochemical and adsorptive properties of activated carbons from Arundo donax Linn utilizing different iron salts as activating agents. J Taiwan Inst Chem Eng 45:3007–3015

Girgis BS, El-Hendawy ANA (2002) Porosity development in activated carbons obtained from date pits under chemical activation with phosphoric acid. Microporous Mesoporous Mater 52:105–117

Gonzalez-Serrano E, Cordero T, Rodriguez-Mirasol J, Cotoruelo L, Rodriguez JJ (2004) Removal of water pollutants with activated carbons prepared from H_3PO_4 activation of lignin from kraft black liquors. Water Res 38:3043–3050

Hesas RH, Arami-Niya A, Daud WMAW, Sahu JN (2013) Preparation and characterization of activated carbon from apple waste by microwave-assisted phosphoric acid activation: application in methylene blue adsorption. BioResources 8:2950–2966

Hong D, Zhou J, Hu C, Zhou Q, Mao J, Qin Q (2019) Mercury removal mechanism of AC prepared by one-step activation with $ZnCl_2$. Fuel 235:326–335

Hotova G, Slovak V, Soares OSGP, Figueiredo JL, Pereira MFR (2018) Oxygen surface groups analysis of carbonaceous samples pyrolysed at low temperature. Carbon 134:255–263

Karpenya AM, Kogan AG, Goncharenok YP (2009) Fabrication of organic synthetic fibre plates using short-fibre textile wastes. Fibre Chem 41:337–340

Kotaiah Naik D, Monika K, Prabhakar S, Parthasarathy R, Satyavathi B (2017) Pyrolysis of sorghum bagasse biomass into bio-char and bio-oil products. J Therm Anal Calorim 127:1277–1289

Kuppireddy SKR, Rashid K, Al Shoaibi A, Srinivasakannan C (2014) Production and characterization of porous carbon from date palm seeds by chemical activation with H_3PO_4: process optimization for maximizing adsorption of methylene blue. Chem Eng Commun 201:1021–1040

Li L, Liu S, Liu J (2011) Surface modification of coconut shell based activated carbon for the improvement of hydrophobic VOC removal. J Hazard Mater 192:683–690

Maneechakr P, Karnjanakom S (2017) Adsorption behaviour of Fe(II) and Cr(VI) on activated carbon: surface chemistry, isotherm, kinetic and thermodynamic studies. J Chem Thermodyn 106:104–112

Mohanty K, Jha M, Meikap BC, Biswas MN (2005) Removal of chromium (VI) from dilute aqueous solutions by activated carbon developed from Terminalia arjuna nuts activated with zinc chloride. Chem Eng Sci 60:3049–3059

Moreno-Castilla C, Lopez-Ramon MV, Carrasco-Marin F (2000) Changes in surface chemistry of activated carbons by wet oxidation. Carbon 38:1995–2001

Nahil MA, Williams PT (2010) Activated carbons from acrylic textile waste. J Anal Appl Pyrolysis 89:51–59

Oliveira LC, Pereira E, Guimaraes IR, Vallone A, Pereira M, Mesquita JP, Sapag K (2009) Preparation of activated carbons from coffee husks utilizing $FeCl_3$ and $ZnCl_2$ as activating agents. J Hazard Mater 165: 87–94

Özhan A, Şahin Ö, Küçük MM, Saka C (2014) Preparation and characterization of activated carbon from pine cone by microwave-induced $ZnCl_2$ activation and its effects on the adsorption of methylene blue. Cellulose 21:2457–2467

Rodríguez-Reinoso F, Molina-Sabio M (1992) Activated carbons from lignocellulosic materials by chemical and/or physical activation: an overview. Carbon 30:1111–1118

Rufford TE, Hulicova-Jurcakova D, Zhu Z, Lu GQ (2011) A comparative study of chemical treatment by $FeCl_3$, $MgCl_2$, and $ZnCl_2$ on microstructure, surface chemistry, and double-layercapacitance of carbons from waste biomass. J Mater Res 25:1451–1459

Şahin Ö, Saka C, Ceyhan AA, Baytar O (2014) Preparation of high surface area activated carbon from Elaeagnus angustifolia seeds by chemical activation with $ZnCl_2$ in one-step treatment and its iodine adsorption. Sep Sci Technol 50:886–891

Sawalha MF, Peralta-Videa JR, Saupe GB, Dokken KM, Gardea-Torresdey JL (2007) Using FTIR to corroborate the identity of functional groups involved in the binding of Cd and Cr to saltbush (Atriplex canescens) biomass. Chemosphere 66:1424–1430

Sen Gupta S, Bhattacharyya KG (2011) Kinetics of adsorption of metal ions on inorganic materials: a review. Adv Colloid Interf Sci 162: 39–58

Shimada N, Kawamoto H, Saka S (2008) Different action of alkali/alkaline earth metal chlorides on cellulose pyrolysis. J Anal Appl Pyrolysis 81:80–87

Shouman MA, Fathy NA, Khedr SA, Attia AA (2013) Comparative biosorption studies of hexavalent chromium ion onto raw and modified palm branches. Adv Phys Chem 2013:1–9

Sing KSW (1985) Reporting physisorption data for gas/solid systems with special reference to the determination of surface area and porosity (Recommendations 1984). Pure Appl Chem 57:603–619

Suksabye P, Thiravetyan P, Nakbanpote W, Chayabutra S (2007) Chromium removal from electroplating wastewater by coir pith. J Hazard Mater 141:637–644

Tazibet S, Velasco LF, Lodewyckx P, Abou M'Hamed D, Boucheffa Y (2018) Systematic study of the role played by $ZnCl_2$ during the carbonization of a chemically activated carbon by TG-MS and DSC. J Therm Anal Calorim 134:1395–1404

Tian D, Xu Z, Zhang D, Chen W, Cai J, Deng H, Sun Z, Zhou Y (2019) Micro-mesoporous carbon from cotton waste activated by $FeCl_3$/$ZnCl_2$: preparation, optimization, characterization and adsorption of methylene blue and eriochrome black T. J Solid State Chem 269:580–587

Vasconcelos A, Cavaco-Paulo A (2006) Enzymatic removal of cellulose from cotton/polyester fabric blends. Cellulose 13:611–618

Villacanas F, Pereira MFR, Orfao JJM, Figueiredo JL (2006) Adsorption of simple aromatic compounds on activated carbons. J Colloid Interface Sci 293:128–136

Wang Y (2010) Fiber and textile waste utilization. Waste Biomass Valor 1:135–143

Wang T, Tan S, Liang C (2009) Preparation and characterization of activated carbon from wood via microwave-induced $ZnCl_2$ activation. Carbon 47:1880–1883

Wang S, Wei M, Xu Q, Jia H (2016) Functional porous carbons from waste cotton fabrics for dyeing wastewater purification. Fibers Polym 17:212–219

Wong S, Lim Y, Ngadi N, Mat R, Hassan O, Inuwa IM, Mohamed NB, Low JH (2018) Removal of acetaminophen by activated carbon synthesized from spent tea leaves: equilibrium, kinetics and thermodynamics studies. Powder Technol 338:878–886

Xing X, Jiang W, Li S, Zhang X, Wang W (2019) Preparation and analysis of straw activated carbon synergetic catalyzed by $ZnCl_2$-H_3PO_4 through hydrothermal carbonization combined with ultrasonic assisted immersion pyrolysis. Waste Manag 89:64–72

Xu Z, Yuan Z, Zhang D, Chen W, Huang Y, Zhang T, Tian D, Deng H, Zhou Y, Sun Z (2018a) Highly mesoporous activated carbon synthesized by pyrolysis of waste polyester textiles and $MgCl_2$: physiochemical characteristics and pore-forming mechanism. J Clean Prod 192:453–461

Xu Z, Zhang T, Yuan Z, Zhang D, Sun Z, Huang Y, Chen W, Tian D, Deng H, Zhou Y (2018b) Fabrication of cotton textile waste-based magnetic activated carbon using $FeCl_3$ activation by the Box-Behnken design: optimization and characteristics. RSC Adv 8: 38081–38090

Xu Z, Sun Z, Zhou Y, Chen W, Zhang T, Huang Y, Zhang D (2019a) Insights into the pyrolysis behavior and adsorption properties of activated carbon from waste cotton textiles by $FeCl_3$-activation. Colloids Surf A Physicochem Eng Asp 582:123934

Xu Z, Yuan Z, Zhang D, Huang Y, Chen W, Sun Z, Zhou Y (2019b) Cr(VI) removal with rapid and superior performance utilizing cost-efficient waste-polyester-textile-based mesoporous carbon: behavior and mechanism. J Mol Liq 278:496–504

Xu Z, Zhou Y, Sun Z, Zhang D, Huang Y, Gu S, Chen W (2020) Understanding reactions and pore-forming mechanisms between waste cotton woven and $FeCl_3$ during the synthesis of magnetic activated carbon. Chemosphere 241:125120

Yahya MA, Al-Qodah Z, Ngah CWZ (2015) Agricultural bio-waste materials as potential sustainable precursors used for activated carbon production: a review. Renew Sust Energ Rev 46:218–235

Yuan P, Fan M, Yang D, He H, Liu D, Yuan A, Zhu J, Chen T (2009) Montmorillonite-supported magnetite nanoparticles for the removal of hexavalent chromium [Cr(VI)] from aqueous solutions. J Hazard Mater 166:821–829

Zhang Y-J, Ou J-L, Duan Z-K, Xing Z-J, Wang Y (2015) Adsorption of Cr(VI) on bamboo bark-based activated carbon in the absence and presence of humic acid. Colloids Surf A Physicochem Eng Asp 481: 108–116

Zheng J, Zhao Q, Ye Z (2014) Preparation and characterization of activated carbon fiber (ACF) from cotton woven waste. Appl Surf Sci 299:86–91

Zhou M, Pu F, Wang Z, Guan S (2014) Nitrogen-doped porous carbons through KOH activation with superior performance in supercapacitors. Carbon 68:185–194

Zhu X, Liu Y, Luo G, Qian F, Zhang S, Chen J (2014) Facile fabrication of magnetic carbon composites from hydrochar via simultaneous activation and magnetization for triclosan adsorption. Environ Sci Technol 48:5840–5848